Plasmon Blockade in Nanostructured Graphene

Alejandro Manjavacas,[†,*] Peter Nordlander,[‡] and F. Javier García de Abajo[†,§,*]

[†]IQFR-CSIC, Serrano 119, 28006 Madrid, Spain and [‡]Department of Physics and Astronomy, M.S. 61, Rice University, Houston, Texas 77005-1892, United States. [§]Present address: Currently on sabbatical at Optoelectronics Research Centre, University of Southampton, Southampton SO17 1BJ, U.K.

ABSTRACT

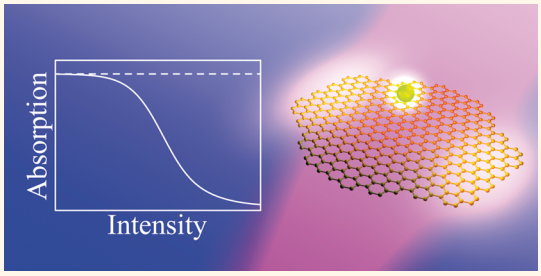

Among the many extraordinary properties of graphene, its optical response allows one to easily tune its interaction with nearby molecules *via* electrostatic doping. The large confinement displayed by plasmons in graphene nanodisks makes it possible to reach the strong-coupling regime with a nearby quantum emitter, such as a quantum dot or a molecule. In this limit, the quantum emitter can introduce a significant plasmon−plasmon interaction, which gives rise to a plasmon blockade effect. This produces, in turn, strongly nonlinear absorption cross sections and modified statistics of the bosonic plasmon mode. We characterize these phenomena by studying the equal-time second-order correlation function $g^{(2)}(0)$, which plunges below a value of 1, thus revealing the existence of nonclassical plasmon states. The plasmon-emitter coupling, and therefore the plasmon blockade, can be efficiently controlled by tuning the doping level of the graphene nanodisks. The proposed system emerges as a new promising platform to realize quantum plasmonic devices capable of commuting optical signals at the single-photon/plasmon level.

KEYWORDS: quantum plasmonics · graphene plasmons · plasmon blockade · nonclassical plasmons · nanophotonics · strong coupling · graphene nanodisk

Controlling light−matter interaction at the nanoscale is one of the paramount goals of nanophotonics,[1−3] which has stimulated a large deal of work in recent years intended to understand and characterize metallic nanostructures that support surface plasmons.[4−8] These excitations are capable of confining light fields in regions well below the diffraction limit, while they simultaneously display large enhancement of the electromagnetic field.[9,10] Because of these properties, surface plasmons have been used in different applications ranging from ultrasensitive biosensing[11,12] to nano-optical circuits.[13] Additionally, the large fields associated with surface plasmons can produce strong interactions with other photonic elements, such as quantum emitters, thus giving rise to new hybrid plasmon-emitter systems exhibiting unique optical response.[14−24]

The possibility of reaching the quantum regime using plasmonic systems faces difficult challenges but offers great opportunities.[25−27] For instance, the nonlinear behavior arising from the quantum nature of both a fermionic emitter and light has been extensively investigated on theoretical and experimental grounds over the past decade.[28,29] An interesting example is the photon blockade effect,[30] which has been experimentally observed in atoms coupled to cavities,[31] as well as in superconducting circuits.[32] The essential ingredient of these experiments is the achievement of strong light−matter coupling, characterized by an interaction energy exceeding the damping introduced by cavity losses. Nonetheless, reaching the strong-coupling regime is a delicate task that has so far been reserved to a handful of cavity quantum electrodynamics (QED) experiments.

The extension of this regime to quantum emitters interacting with plasmons supported by metallic nanoparticles has been recently pursued[20−24] in order to realize quantum behavior in more robust and compact systems than the elaborate QED setups. However, this goal seems to be very difficult to achieve using standard plasmonic materials such as noble metals due to the relatively large losses inherent in these materials, which limit the lifetime of the plasmons to ∼10 optical cycles. A promising alternative approach consists of using plasmons supported by doped graphene nanodisks, which have recently been shown to be capable of producing strong coupling[33] as a consequence of their longer lifetimes (∼100 optical cycles[34]). A rich variety of graphene plasmons have been investigated[33−36] that should allow the manipulation of plasmon propagation and trapping.

* Address correspondence to a.manjavacas@csic.es, j.g.deabajo@csic.es.

Received for review December 3, 2011 and accepted January 6, 2012.

Published online January 06, 2012
10.1021/nn204701w

© 2012 American Chemical Society

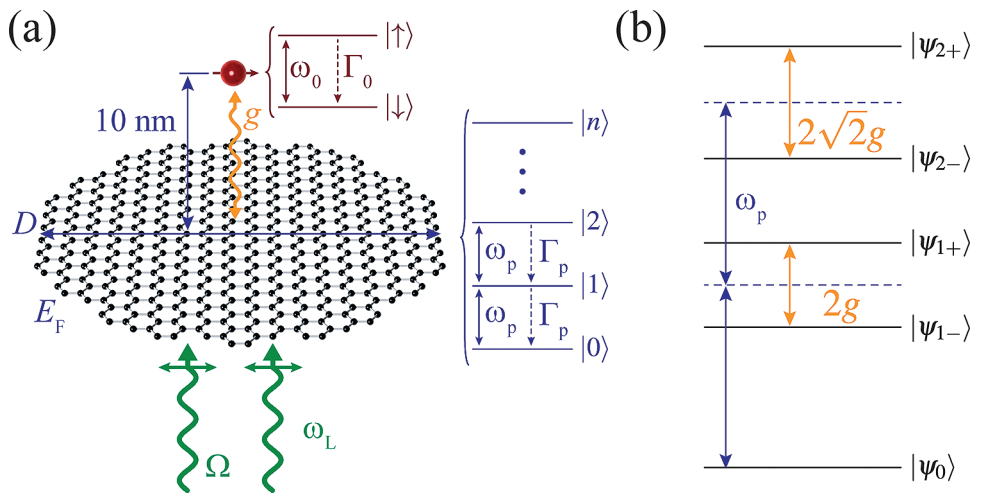

Figure 1. Description of the graphene-nanodisk/emitter combined system under study. (a) A quantum emitter is placed 10 nm above a doped graphene nanodisk of diameter *D* and Fermi energy E_F. The disk can support localized surface plasmons of frequency ω_p and lifetime Γ_p^{-1}. The quantum emitter is described as a two-level system (ground state $|\downarrow\rangle$ and excited state $|\uparrow\rangle$, transition frequency ω_0, excited-state lifetime Γ_0^{-1}). The dipole moment of the quantum emitter, taken to be parallel to the disk, interacts with the near field of the graphene plasmon with effective coupling strength *g*. The entire system is illuminated by an external laser of frequency ω_L and intensity quantified in terms of the Rabi frequency Ω. (b) Energy level diagram of the interacting system for $\omega_0 = \omega_p$. The energy diagrams of (a) correspond to the noninteracting disk and emitter, in which the energy level spacing is constant. In contrast, the spacings between the interacting levels in (b) are different as a result of the coupling between the emitter and the graphene plasmon. This interaction introduces anharmonicity and nonlinearity in the optical response.

The very small plasmon damping in graphene is caused by the extraordinary electrical properties of single-layer carbon,[37−39] which together with the possibility of modifying the plasmonic spectrum of graphene nanostructures *via* doping[40] opens new paths for developing quantum plasmonic devices capable of controlling light−matter interaction at the quantum level.

In this article, we show that quantum effects can introduce a strong nonlinear optical response in a system formed by a doped graphene nanodisk and a nearby quantum emitter. We predict a plasmon blockade effect under feasible conditions, which allows actively switching the optical properties of the resulting device in a manner analogous to the photon blockade effect that has been extensively studied in cooled atoms coupled to photonic cavities. We show that, in contrast to photon blockade, the wavelength at which plasmon blockade takes place can be straightforwardly tuned simply by changing the charge in the graphene *via* electrostatic gating.[41] The plasmon blockade effect produces nonclassical distributions when multiple plasmon states are generated. Our study emphasizes nanostructured graphene coupled to quantum emitters as a viable platform to implement quantum information devices in robust, tunable structures.

The system under study is depicted in Figure 1. We consider a graphene nanodisk of diameter *D* doped to a Fermi energy E_F relative to the Fermi energy for the neutral disk. This graphene nanostructure supports localized surface plasmons[33] of energy $\hbar\omega_p$. Specifically, we focus on a dipolar plasmon with polarization parallel to the disk and $m = 1$ azimuthal symmetry. The quantum emitter, which is placed 10 nm above the nanodisk, is described as a two-level system with excited and ground states $|\uparrow\rangle$ and $|\downarrow\rangle$ separated by an energy $\hbar\omega_0$. The entire system is illuminated by an external laser of frequency ω_L. In the absence of any losses, the dynamical evolution of the interacting system can be described by a Hamiltonian that consists of three terms: $H = H_{free} + H_{int} + H_{ext}$. The first, which describes the evolution of the noninteracting system, reads

$$H_{free} = \hbar\omega_p a^\dagger a + \hbar\omega_0 \sigma^\dagger \sigma \quad (1)$$

where a and $\sigma = |\downarrow\rangle\langle\uparrow|$ ($a^\dagger$ and $\sigma^\dagger = |\uparrow\rangle\langle\downarrow|$) are the annihilation (creation) operators for the graphene plasmon and the excited state of the emitter, respectively. The coupling between the two excitations is described by the second term

$$H_{int} = \hbar g(a^\dagger \sigma + a\sigma^\dagger) \quad (2)$$

where g is a coupling constant that determines the strength of the interaction. The last term accounts for the effect of the laser

$$H_{ext} = \hbar\Omega e^{-i\omega_L t} a^\dagger + \hbar\Omega^* e^{i\omega_L t} a \quad (3)$$

which operates at frequency ω_L with an intensity defined in terms of the Rabi frequency Ω. In this expression, we have neglected direct pumping of the emitter because its cross section is generally several orders of magnitude smaller than the one of the graphene plasmon.

We incorporate dissipation *via* the master equation for the density operator[42] $\dot{\rho} = \mathscr{L}(\rho)$, where the Liovillian[43] $\mathscr{L}$ is given by

$$\mathscr{L}(\rho) = \frac{i}{\hbar}[\rho, H] + \mathscr{L}_0(\rho) + \mathscr{L}_p(\rho) \quad (4)$$

The first term of this expression contains the Hamiltonian and determines the coherent evolution of the system, while the Lindblad terms[43] $\mathcal{L}_i(\rho) = \Gamma_i/2[2c_i\rho c_i^\dagger - \rho c_i^\dagger c_i - c_i^\dagger c_i\rho]$, with $i = 0, p$, account for the damping of both the excited emitter state ($c_0 = \sigma$) and the graphene plasmon ($c_p = a$).

RESULTS AND DISCUSSION

Plasmon Blockade. Apart from the coupling to external light, H is the well-known Jaynes–Cummings Hamiltonian,[44] which has the same ground state as H_{free} $|\psi_0\rangle = |\downarrow 0\rangle$, and whose excited states $|\psi_{n\pm}\rangle$ are pairs of linear combinations of $|\uparrow n-1\rangle$ and $|\downarrow n\rangle$, where n is the plasmon occupation number, with eigenenergies

$$E_{n\pm} = \hbar\left(n\omega_p + \frac{\delta}{2} \pm \sqrt{\frac{\delta^2}{4} + ng^2}\right) \quad (5)$$

where $\delta = \omega_0 - \omega_p$ (see Supporting Information). In each pair of states, the sum of the number of plasmon and emitter excitations is n. As we show in Figure 1b, the interaction of the plasmon with the two-level emitter results in a nonuniform distribution of states known as Jaynes–Cummings ladder,[45] in which the states of each pair are separated by an energy determined by the emitter-plasmon coupling g, the detuning δ, and the quantum occupation number n. The resulting nonlinear dependence of the excitation energy on n is equivalent to anharmonicity and has an important consequence: an external light source tuned to be resonant with the plasmon frequency ω_p becomes increasingly more detuned as the system climbs the energy ladder and n increases. The detuning with respect to the uncoupled plasmon frequency is given by $(E_{(n+1)\pm} - E_{n\pm})/\hbar - \omega_p = \pm((\delta^2/4 + (n+1)g^2)^{1/2} - (\delta^2/4 + ng^2)^{1/2})$, which is maximum for $\delta = 0$ (*i.e.*, $\omega_0 = \omega_p$). An increasing detuning obviously limits the possibility of generating an arbitrary number of plasmons. We refer to this behavior as plasmon blockade, in direct analogy to the so-called photon blockade observed in cavity QED experiments.[31]

It is important to notice that the nonlinear behavior associated with the plasmon blockade is only effective in systems for which the coupling g dominates over the losses Γ_p and Γ_0. In general, plasmonic losses are several orders of magnitude larger than quantum emitter losses ($\Gamma_p \gg \Gamma_0$), and thus the condition for observation of an efficient plasmon blockade amounts to $g/\Gamma_p \gg 1$. This is known as strong-coupling regime, which is difficult to reach using plasmons supported by standard metallic nanostructures.[16−24] However, the coupling strength g/Γ_p associated with the dipolar plasmon of a graphene nanodisk of diameter D = 100 nm reaches values in the 1.5−3 range for moderate Fermi energies E_F = 0.2−0.6 eV, and it decreases for larger D. Here, we assume typical values for the quantum emitter natural decay rate $\Gamma_0 = 5 \times 10^7$ s^{-1}, the nanodisk diameters D = 100−200 nm, and the Fermi energies E_F = 0.2−0.6 eV, for which the plasmon energy and width take values $\hbar\omega_p \approx$ 0.1−0.25 eV and $\hbar\Gamma_p \approx$ 1−3.5 meV (see Methods for more details on the calculation of ω_p and Γ_p and their dependence on D and E_F).

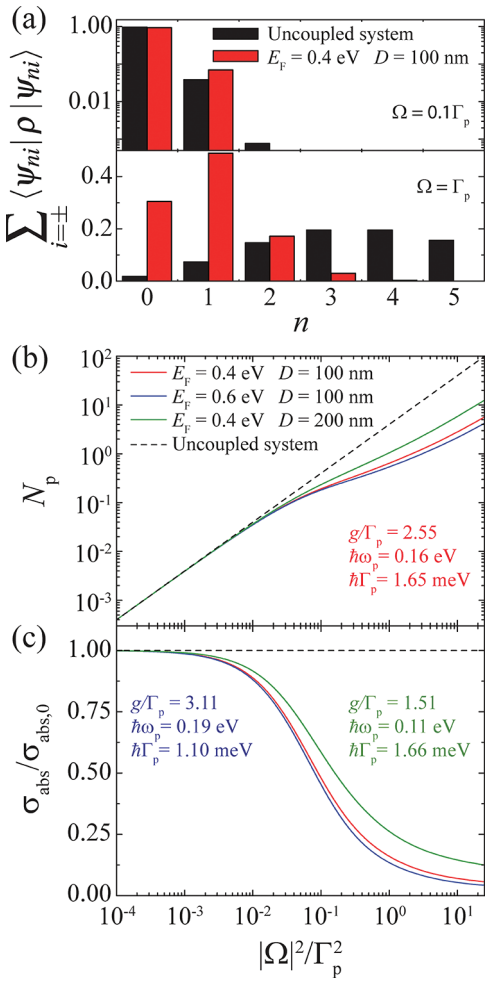

Figure 2. Plasmon blockade. (a) Population of the different states of a graphene-nanodisk/emitter system for two different values of the external laser intensity under continuous illumination conditions. Results for interacting (g/Γ_p = 2.55, red) and noninteracting (g/Γ_p = 0, black) systems are contrasted. We assume resonant coupling ($\omega_0 = \omega_p$) and tune the laser frequency to the $|\psi_0\rangle \rightarrow |\psi_{1+}\rangle$ transition. For this laser frequency, only $|\psi_{n+}\rangle$ states are significantly populated in the interacting system. (b) Average number of plasmons in the graphene nanodisk N_p as a function of laser intensity for different disk diameters D and Fermi energies E_F (solid curves) under the same conditions as in (a). The uncoupled system (dashed line) shows a linear increase of N_p with the laser intensity. In contrast, the coupled system (solid curves) exhibits a clear nonlinear behavior for $|\Omega|^2/\Gamma_p^2 > 10^{-2}$. The nonlinearity is more pronounced for larger graphene-nanodisk/emitter coupling g (cf. red, blue, and green curves). (c) Absorption cross section of the graphene-nanodisk/emitter coupled system normalized to the value of the uncoupled configuration as a function of laser intensity. A departure from the linear regime is observed for large laser intensities.

Figure 2 shows some of the main signatures of plasmon blockade in the nanodisk-emitter systems. In what follows, we present results for steady-state

conditions under continuous wave illumination. In particular, Figure 2a shows the population of different state pairs n under stationary conditions. We consider two different illumination intensities ($|\Omega|^2 = 0.01\Gamma_p^2$ and $|\Omega|^2 = \Gamma_p^2$), take $\omega_0 = \omega_p$, and tune the laser frequency to be resonant with the $|\psi_0\rangle \rightarrow |\psi_{1+}\rangle$ transition. The black bars are the results for the uncoupled system (*i.e.*, in the absence of the quantum emitter), while the red bars refer to the interacting system with a coupling constant $g = 2.55\Gamma_p$. For low illumination intensities (upper part), the ground state ($n = 0$) takes most of the weight, while the first excited states ($n = 1$) are only marginally populated. In contrast, for high intensity (lower part), the population of the system is distributed among different excited states but with very different profiles for configurations with and without coupling. For the uncoupled system, the population follows a broad Poisson distribution centered around $n = 4$, but for the coupled system, the population is mainly concentrated in the ground ($n = 0$) and singly excited ($n = 1$) states. This is a direct consequence of the nonlinearity and anharmonicity associated with the plasmon blockade, which prevents efficient plasmon excitation beyond $n = 1$.

In Figure 2b, we show the average number of plasmons $N_p = \langle a^\dagger a\rangle$ supported by the graphene nanodisks as a function of external illumination intensity for different values of E_F and D (solid curves). The corresponding calculated coupling constant (g, see Methods), plasmon frequency, and decay rate (ω_p and Γ_p) are shown in the text insets throughout Figure 2b,c with color codes standing for the selected values of E_F and D. Obviously, the uncoupled system ($g = 0$) presents a linear dependence on intensity, $N_p = 4|\Omega|^2/\Gamma_p^2$ (dashed curve, plotted for reference). In contrast, a significant departure from this linear behavior is observed above $|\Omega|^2/\Gamma_p^2 \approx 10^{-2}$ in the coupled system as a signature of plasmon blockade (solid curves). As expected, the nonlinearity increases with g. In the small intensity limit, the linear behavior is recovered for any value of g, as N_p is well below 1 (*e.g.*, for $|\Omega|^2/\Gamma_p^2 < 10^{-2}$). However, even in this limit, the plasmon blockade severely modifies the plasmon statistics, as we show below.

The normalized absorption cross section is shown in Figure 2c as computed by assuming that the dominant dissipation channel is inelastic plasmon decay, and that the radiative part represents only a small fraction, $\lesssim$1%, of the total decay rate.[46] In this limit, the absorption cross section can be written as $\sigma_{abs} = \hbar\omega_p\Gamma_p N_p/I$, where $I \propto |\Omega|^2$ is the laser intensity (see Methods for the explicit dependence of I on $|\Omega|^2$). It is convenient to normalize the cross section to that of the uncoupled graphene disk $\sigma_{abs,0}$ as

$$\frac{\sigma_{abs}}{\sigma_{abs,0}} = \frac{N_p}{4}\frac{\Gamma_p^2}{|\Omega|^2} \qquad (6)$$

As shown in Figure 2c, the normalized absorption decreases with increasing intensity and the nanodisk-emitter system behaves as a saturable absorber, again as a result of plasmon blockade, which is more pronounced for larger g (cf. green and blue curves).

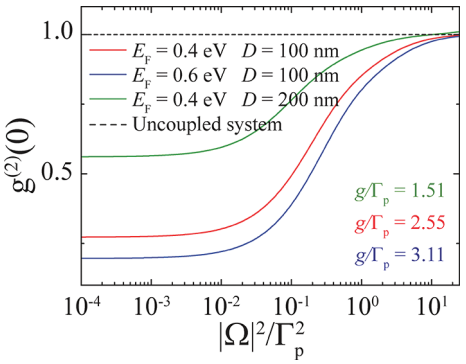

Figure 3. Nonclassical plasmon states. We show the equal-time second-order correlation function $g^{(2)}(0) = \langle a^\dagger a^\dagger aa\rangle/N_p^2$ *versus* laser intensity for different disk diameters D and Fermi energies E_F (solid curves) under the same conditions as in Figure 2. We also show $g^{(2)}(0) = 1$ (dashed line), as obtained for the uncoupled system. For finite coupling (solid curves) and relatively low intensity, $g^{(2)}(0)$ lies below 1 and decreases with increasing g/Γ_p, thus revealing the creation of nonclassical plasmon states. For large intensity, $g^{(2)}(0)$ increases and eventually becomes larger than 1.

Nonclassical Plasmons. Besides the plasmon blockade effect, the coupling between a graphene plasmon and a quantum emitter can also produce strong modifications in the plasmon statistics, which we characterize through the equal-time second-order correlation function, defined as[47] $g^{(2)}(0) = \langle a^\dagger a^\dagger aa\rangle/N_p^2$. This quantity becomes 1 for Poissonian distributions (also known as coherent states), which also characterize photons in a coherent laser source. In contrast, $g^{(2)}(0) > 1$ is associated with thermal distributions (super-Poissonian statistics), leading to bunching of photon pairs emerging from a thermal source (similar bunching is expected in thermally excited plasmons in uncoupled nanodisks). However, it is only for $g^{(2)}(0) < 1$ (sub-Poissonian statistics, leading to antibunching[48]) that a quantum description of photons or plasmons is needed, as a classical model cannot produce these values of the correlation function. Indeed, $g^{(2)}(0) = 0$ would mean the existence of a single plasmon state.

For graphene nanodisk plasmons, $g^{(2)}(0)$ can be directly measured from the photons emitted *via* radiative plasmon decay.[26] Although less than one in a hundred plasmons decays by emitting a photon,[33] even for the smallest intensities of the external illumination under consideration the resulting photon flux should allow for experimental verification of the nonclassical, quantum plasmonic regime: for instance, for a moderate incident intensity $\Omega = 0.1\Gamma_p$, the rate of photon generation $\approx N_p\Gamma_{p,rad} \approx 4 \times 10^{-4}\Gamma_p \approx 10^9\ s^{-1}$ is significant.

Figure 3 shows $g^{(2)}(0)$ as a function of laser intensity for the different graphene nanodisks discussed in Figure 2. We assume that the laser frequency is

resonant with the $|\psi_0\rangle \rightarrow |\psi_{1+}\rangle$ transition, and $\omega_0 = \omega_p$. In the absence of a quantum emitter (uncoupled system), we have $g^{(2)}(0) = 1$ (dashed line), so that plasmons are generated in coherent states, which are typical of coherent classical systems. When coupling is switched on (solid curves), $g^{(2)}(0)$ drops below 1, and thus, nonclassical plasmon states are generated. Furthermore, the minimum value that is reached depends on the coupling strength, decreasing with increasing g. As the laser intensity grows, $g^{(2)}(0)$ approaches the classical threshold $g^{(2)}(0) = 1$ and eventually rises above this value. This behavior can be understood by examining Figure 2a, in which we see that small values of $|\Omega|^2/\Gamma_p^2$ produce a negligible population of states above $n = 1$, therefore resulting in sub-Poissonian statistics. In contrast, for larger intensities, the population of $n > 1$ states increases, thus resulting in the super-Poissonian behavior shown in Figure 3 despite the plasmon blockade.

Tunability of Plasmon Blockade. A great advantage of the plasmons supported by the graphene nanodisks is the possibility of controlling their properties by tuning the Fermi energy. This can be achieved, for instance, by introducing electrostatic doping,[40] thus allowing us the tuning of both the plasmon energy and its coupling with the quantum emitter, and by extension, the modulation of the plasmon blockade effect. This is illustrated in Figure 4a, which shows the normalized absorption cross section defined by eq 6 as a function of the graphene Fermi energy for different values of the laser intensity. The excitation energy of the quantum emitter is set to 0.16 eV, which coincides with the plasmon energy for $E_F = 0.4$ eV. As in the remainder of this work, the laser frequency is chosen to be resonant with the $|\psi_0\rangle \rightarrow |\psi_{1+}\rangle$ transition.

At small intensities (red curve), the normalized absorption cross section approximately follows the same behavior as in the uncoupled system (dashed line), with a slight departure for low Fermi energies. When $|\Omega|^2$ increases (blue and green curves), the plasmon blockade effect produces significant nonlinearity. The nonlinearity is stronger for E_F below the resonance condition $E_F = 0.4$ eV. This behavior is directly connected to the evolution of $|\psi_{n\pm}\rangle$ states with detuning δ: these states are linear combinations of $|\uparrow n-1\rangle$ and $|\downarrow n\rangle$, but absorption dominates in the latter because it contains a larger number of plasmons. More precisely, the external illumination is tuned to induce transitions from the ground state to $|\psi_{1+}\rangle$. For $E_F > 0.4$ eV (*i.e.*, $g < |\delta|$ and $\delta < 0$), one finds that $|\downarrow 1\rangle$ has stronger weight in $|\psi_{1+}\rangle$ (see Supporting Information), thus leading to higher absorption. In contrast, for $E_F < 0.4$ eV, where $g < |\delta|$ and $\delta > 0$, the weight of $|\downarrow 1\rangle$ is smaller and absorption is reduced. This example clearly illustrates that it is possible to enhance plasmon blockade by detuning the plasmon energy, which of course can be controlled *via* the Fermi energy of the graphene nanodisk, provided we have coupling to a quantum emitter.

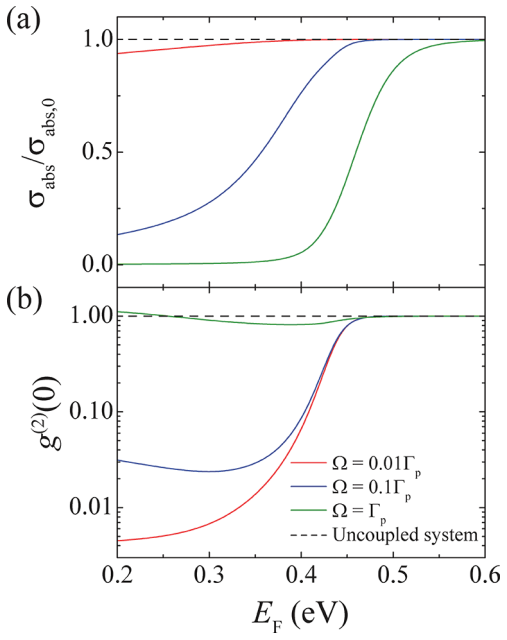

Figure 4. Tunability of graphene-nanodisk/emitter systems. (a) Normalized absorption cross section of a graphene-nanodisk/emitter system as a function of graphene Fermi energy for different values of the external laser intensity. The nanodisk diameter is $D = 100$ nm. The emitter has fixed excitation energy $\hbar\omega_0 = 0.16$ eV, which coincides with the plasmon energy $\hbar\omega_p$ for $E_F = 0.4$ eV. We tune the laser frequency to be resonant with the $|\psi_0\rangle \rightarrow |\psi_{1+}\rangle$ transition. The cross section is normalized to that of the uncoupled system. At low laser intensity (red curve), the cross sections with and without coupling are very similar. As $|\Omega|^2$ increases (blue and green curves), the cross section becomes strongly nonlinear for small E_F and essentially linear for large E_F. The transition between these two regimes is sharper for larger laser intensity. (b) Equal-time second-order correlation function $g^{(2)}(0)$ under the same conditions as in (a). For large intensity, $g^{(2)}(0)$ is found to be close to the classical value $g^{(2)}(0) = 1$. When the intensity decreases, we again observe two different regimes: for small E_F, the system exhibits sub-Poissonian statistics associated with the existence of nonclassical plasmons, while for larger E_F, a classical behavior is recovered.

The enhancement of the plasmon blockade also influences the statistics of the generated plasmons, as shown in Figure 4b, where $g^{(2)}(0)$ is plotted as a function of the Fermi energy for the same conditions as in Figure 4a. The dashed line represents the uncoupled system (classical states). In the coupled system (solid curves), we again observe two different regions: for large values of E_F, the system approaches the classical limit ($g^{(2)}(0) \rightarrow 1$) due to the reduction in the efficiency of plasmon blockade. In contrast, for small E_F, the plasmon blockade is enhanced, giving rise to antibunching ($g^{(2)}(0) < 1$). Clearly, the antibunching increases when the Fermi energy becomes smaller than $E_F = 0.4$ eV, where the plasmon and the laser are on resonance. As expected, this effect is more pronounced for smaller illumination intensities (see also Figure 3).

Interestingly, there is an optimum value of E_F for which $g^{(2)}(0)$ reaches a minimum as a result of the interplay between the plasmon-emitter coupling g and

the detuning δ. When the latter increases for $E_F < 0.4$ eV, the state $|\psi_{1+}\rangle$ approaches $|\uparrow 0\rangle$, thus preventing higher n states to be populated, which results in lower $g^{(2)}(0)$. However, at the same time, g decreases, therefore reducing the anharmonicity of the energy ladder, which contributes to increasing the value of $g^{(2)}(0)$. The trade-off between these two effects results in an optimum value of E_F at which $g^{(2)}(0)$ presents a minimum.

CONCLUSIONS

In summary, we have fully characterized the nonlinear optical response of a graphene nanodisk coupled to a quantum emitter. Because of the extraordinarily large lifetimes of graphene plasmons, this system is capable of reaching the strong-coupling regime, where a plasmon blockade effect emerges naturally in its optical response. This effect has two important consequences: (i) the optical absorption cross section is dramatically modified and becomes strongly nonlinear for large illumination intensities; and (ii) the correlation of the generated plasmons exhibits a clear nonclassical behavior, as we demonstrate by studying the equal-time second-order correlation function $g^{(2)}(0)$. More precisely, nonclassical plasmonic states (*i.e.*, states for which $g^{(2)}(0) < 1$) are generated due to the plasmon blockade, an effect that could be possibly detected by measuring correlations of photons emitted by radiative decay. Interestingly, we show that it is possible to control the optical nonlinearity of the graphene nanodisk/emitter system by tuning the plasmonic spectrum of the graphene nanodisk *via* electrostatic doping. Our work opens new paths for the design of novel quantum plasmonic devices with applications ranging from active metamaterials to quantum information processing.

METHODS

Optical Response of Graphene Nanodisks. The optical response of graphene nanodisks has been characterized in previous works.[33,46] Here we follow the same methodology, consisting of rigorously solving Maxwell's equations using the boundary element method (BEM).[49] For our purposes, the nanodisks are parametrized as thin films of thickness t with rounded edges and dielectric function $\varepsilon = 1 + 4\pi i\sigma/\omega t$. We use $t = 0.5$ nm, which is well converged with respect to the $t \to 0$ limit for the disk diameters under consideration. The conductivity $\sigma(\omega)$ is taken from the local limit of the random-phase approximation for an extended graphene sheet[50,51] (see ref 33 and its Supporting Information for more details). Furthermore, we assume an intrinsic relaxation time $\tau = \mu E_F/ev_F^2$, where $v_F \approx c/300$ is the Fermi velocity and $\mu = 10\,000$ cm^2/(V·s) is the measured dc mobility.[37] We extract the plasmon energies $\hbar\omega_p$ and widths $\hbar\Gamma_p$ by fitting the plasmon peak of the numerically calculated absorption spectra to a Lorentzian. This classical description has been proved[52] to be accurate enough and well reproduced by *ab initio* calculations for the dimensions under consideration, with nanodisk diameters larger than 40 nm.

The coupling constant g requires a more elaborate treatment. In the classical limit, the decay rate of a quantum emitter placed close to the graphene nanodisk is given by the expression[1]

$$\Gamma = \Gamma_0 + \frac{2}{\hbar}\,\mathrm{Im}\{\mu_0^* \cdot \mathbf{E}_{\mathrm{ind}}\} \tag{7}$$

where Γ_0 is the free-space decay rate, μ_0 is the quantum emitter dipole moment, and $\mathbf{E}_{\mathrm{ind}}$ is the field self-induced by the emitter due to the presence of the graphene nanodisk. We obtain Γ through the calculation of the self-induced field generated by a dipole and evaluated at its own position. This calculation, which involves the rigorous solution of Maxwell's equations, is performed using BEM. Now, it is clear that this value of Γ must be equal to the emitter decay rate computed from the quantum model in the limit of weak coupling (*i.e.*, $g/\Gamma_p \to 0$). In such limit, we have $|\psi_{1-}\rangle \to |\uparrow 0\rangle$, and therefore $\Gamma \approx \mathrm{Im}\{E_{1-}\}$ becomes (see Supporting Information)

$$\Gamma \approx \Gamma_0 + \frac{4g^2}{\Gamma_p} \tag{8}$$

and finally, we obtain the coupling parameter g by comparing eqs 7 and 8.

Figure S1 in the Supporting Information shows the relevant graphene nanodisk parameters as a function of disk diameter D and Fermi energy E_F. The plasmon energies lie in the 0.10−0.25 eV range for the diameters and Fermi energies considered in this work, while the decay rates lie in the 1.0−3.5 meV range. It is interesting to note that the plasmon decay rate is almost independent of diameter. Finally, the values of the normalized coupling constant g/Γ_p lie always above 1, indicating that the graphene-nanodisk/emitter systems under consideration are in the strong-coupling regime. Furthermore, for the parameters used in this paper, the crossover from the strong to the weak coupling regimes takes place when the separation between the quantum emitter and the graphene nanodisk is on the order of a few tens of nanometers. The preservation of the strong-coupling regime to such large separations, which is a consequence of the narrowness and strength of graphene plasmons, makes it possible to use optical or electrostatic trapping to place the quantum emitter in close proximity to the graphene nanostructure, thus avoiding the undesired effects of coupling to a substrate or electron−hole excitations of the carbon sheet that can be an efficient source of quantum decoherence. Alternatively, a passive dielectric spacer could be used in which case the graphene disk parameters would have to be tuned slightly to accommodate for the plasmon red shift and reduced emitter coupling strength g.

Plasmon Dipole Moment and Rabi Frequency. The polarizability of a graphene disk can be accurately modeled using the following expression[46]

$$\alpha(\omega) = \frac{3c^3\Gamma_{p,\mathrm{rad}}}{2\omega_p^2}\,\frac{1}{\omega_p^2 - \omega^2 - i\Gamma_p\omega^3/\omega_p^2} \tag{9}$$

where ω_p is the plasmon frequency, and $\Gamma_{p,\mathrm{rad}}$ and Γ_p are the radiative and the total plasmon decay rates, respectively. Furthermore, the polarizability associated with the plasmon resonance can also be written as[33]

$$\alpha(\omega) \approx \frac{\mu_p^2}{\hbar\omega_p - \hbar\omega - i\hbar\Gamma_p/2} \tag{10}$$

where μ_p is the dipole moment of the graphene plasmon, which can be determined by comparing this expression with eq 9 for $\omega = \omega_p$. From here, we obtain

$$\mu_p^2 = \frac{3}{4}\hbar\Gamma_{p,\mathrm{rad}}\left(\frac{c}{\omega_p}\right)^3 \tag{11}$$

The Rabi frequency is defined as

$$\Omega = \frac{\mu_p E}{\hbar} \tag{12}$$

where E is the electric-field amplitude corresponding to an external illumination intensity $I = [c/(2\pi)]E^2$. Using eq 11, we can relate the Rabi frequency to the intensity as

$$I = \frac{2c\hbar}{3\pi}\left(\frac{\Gamma_p^2}{\Gamma_{p,\,rad}}\right)\frac{\omega_p^3}{c^3}\left(\frac{\Omega}{\Gamma_p}\right)^2 \qquad (13)$$

We need to know ω_p, Γ_p, and $\Gamma_{p,rad}$ in order to evaluate this expression. The first two of these parameters can be obtained as explained in the previous section, and we find $\Gamma_{p,rad}$ by fitting the extinction cross section calculated from BEM to $\sigma_{ext} = (4\pi\omega/c)\mathrm{Im}\{\alpha(\omega)\}$, with $\alpha(\omega)$ given by eq 9.

Figure S2a in the Supporting Information shows the plasmon radiative decay rate normalized to the total decay rate as a function of disk diameter D for three different values of the Fermi energy (E_F = 0.2, 0.4, and 0.6 eV). Radiative decay systematically amounts for less than 1% of the total decay. Finally, we show in Figure S2b the Rabi frequency calculated from eq 13 using these results for $\Gamma_{p,rad}$. Incidentally, the Rabi frequencies considered in Figure 2 of this article lie in the $\Omega = 0.01\Gamma_p - 5\Gamma_p$ range, which corresponds to moderate laser intensities extending from I = 96 W/m^2 to $I = 1.3 \times 10^8$ W/m^2.

Acknowledgment. This work has been supported by the Spanish MICINN (MAT2010-14885 and Consolider NanoLight.es) and the European Commission (FP7-ICT-2009-4-248909-LIMA and FP7-ICT-2009-4-248855-N4E). A.M. acknowledges financial support through FPU from the Spanish ME. P.N. acknowledges support from the Robert A. Welch Foundation under Grant C-1222 and the Center for Solar Photophysics, an Energy Frontier Research Center funded by the U.S. Department of Energy.

Supporting Information Available: We provide additional information of eigenstates and eigenenergies of the Jaynes–Cummings Hamiltonian, together with figures of the relevant parameters of our model. This material is available free of charge *via* the Internet at http://pubs.acs.org.

REFERENCES AND NOTES

1. Novotny, L.; Hecht, B. *Principles of Nano-Optics*; Cambridge University Press: New York, 2006.
2. Pasquale, A. J.; Reinhard, B. M.; Negro, L. D. Engineering Photonic–Plasmonic Coupling in Metal Nanoparticle Necklaces. *ACS Nano* **2011**, *5*, 6578–6585.
3. Zhao, J.; Frank, B.; Burger, S.; Giessen, H. Large-Area High-Quality Plasmonic Oligomers Fabricated by Angle-Controlled Colloidal Nanolithography. *ACS Nano* **2011**, *5*, 9009–9016.
4. Maier, S. A. *Plasmonics: Fundamentals and Applications*; Springer: New York, 2007.
5. Juluri, B. K.; Chaturvedi, N.; Hao, Q.; Lu, M.; Velegol, D.; Jensen, L.; Huang, T. J. Scalable Manufacturing of Plasmonic Nanodisk Dimers and Cusp Nanostructures Using Salting-Out Quenching Method and Colloidal Lithography. *ACS Nano* **2011**, *5*, 5838–5847.
6. Duan, H.; Hu, H.; Kumar, K.; Shen, Z.; Yang, J. K. W. Direct and Reliable Patterning of Plasmonic Nanostructures with Sub-10-nm Gaps. *ACS Nano* **2011**, *5*, 7593–7600.
7. Chen, H.; Shao, L.; Ming, T.; Woo, K. C.; Man, Y. C.; Wang, J.; Lin, H.-Q. Observation of the Fano Resonance in Gold Nanorods Supported on High-Dielectric-Constant Substrates. *ACS Nano* **2011**, *5*, 6754–6763.
8. Van Dorpe, P.; Ye, J. Semishells: Versatile Plasmonic Nanoparticles. *ACS Nano* **2011**, *5*, 6774–6778.
9. Halas, N. J.; Lal, S.; Chang, W.-S.; Link, S.; Nordlander, P. Plasmons in Strongly Coupled Metallic Nanostructures. *Chem. Rev.* **2011**, *111*, 3913–3961.
10. Aubry, A.; Lei, D. Y.; Maier, S. A.; Pendry, J. B. Plasmonic Hybridization Between Nanowires and a Metallic Surface: A Transformation Optics Approach. *ACS Nano* **2011**, *5*, 3293–3308.
11. Álvarez-Puebla, R. A.; Liz-Marzán, L. M.; García de Abajo, F. J. Light Concentration at the Nanometer Scale. *J. Phys. Chem. Lett.* **2010**, *1*, 2428–2434.
12. Taylor, R. W.; Lee, T.-C.; Scherman, O. A.; Esteban, R.; Aizpurua, J.; Huang, F. M.; Baumberg, J. J.; Mahajan, S. Precise Subnanometer Plasmonic Junctions for SERS within Gold Nanoparticle Assemblies Using Cucurbit[n]uril "Glue". *ACS Nano* **2011**, *5*, 3878–3887.
13. Ozbay, E. Plasmonics: Merging Photonics and Electronics at Nanoscale Dimensions. *Science* **2006**, *311*, 189–193.
14. Banerjee, P.; Conklin, D.; Nanayakkara, S.; Park, T.-H.; Therien, M. J.; Bonnell, D. A. Plasmon-Induced Electrical Conduction in Molecular Devices. *ACS Nano* **2010**, *4*, 1019–1025.
15. Zheng, Y. B.; Yang, Y.-W.; Jensen, L.; Fang, L.; Juluri, B. K.; Flood, A. H.; Weiss, P. S.; Stoddart, J. F.; Huang, T. J. Active Molecular Plasmonics: Controlling Plasmon Resonances with Molecular Switches. *Nano Lett.* **2009**, *9*, 819–825.
16. Zhang, W.; Govorov, A. O.; Bryant, G. W. Semiconductor-Metal Nanoparticle Molecules: Hybrid Excitons and the Nonlinear Fano Effect. *Phys. Rev. Lett.* **2006**, *97*, 146804.
17. Artuso, R. D.; Bryant, G. W. Optical Response of Strongly Coupled Quantum Dot-Metal Nanoparticle Systems: Double Peaked Fano Structure and Bistability. *Nano Lett.* **2008**, *8*, 2106–2111.
18. Savasta, S.; Saija, R.; Ridolfo, A.; Di Stefano, O.; Denti, P.; Borghese, F. Nanopolaritons: Vacuum Rabi Splitting with a Single Quantum Dot in the Center of a Dimer Nanoantenna. *ACS Nano* **2010**, *4*, 6369–6376.
19. Wu, X.; Gray, S. K.; Pelton, M. Quantum-Dot-Induced Transparency in a Nanoscale Plasmonic Resonator. *Opt. Express* **2010**, *18*, 23633–23645.
20. Artuso, R. D.; Bryant, G. W. Strongly Coupled Quantum Dot–Metal Nanoparticle Systems: Exciton-Induced Transparency, Discontinuous Response, and Suppression as Driven Quantum Oscillator Effects. *Phys. Rev. B* **2010**, *82*, 195419.
21. Ridolfo, A.; Di Stefano, O.; Fina, N.; Saija, R.; Savasta, S. Quantum Plasmonics with Quantum Dot–Metal Nanoparticle Molecules: Influence of the Fano Effect on Photon Statistics. *Phys. Rev. Lett.* **2010**, *105*, 263601.
22. Kyas, G.; May, V. Density Matrix Based Microscopic Theory of Molecule Metal–Nanoparticle Interactions: Linear Absorbance and Plasmon Enhancement of Intermolecular Excitation Energy Transfer. *J. Chem. Phys.* **2011**, *134*, 034701.
23. Manjavacas, A.; García de Abajo, F. J.; Nordlander, P. N. Quantum Plexcitonics: Strongly Interacting Plasmons and Excitons. *Nano Lett.* **2011**, *11*, 2318–2323.
24. Zhang, W.; Govorov, A. O. Quantum Theory of the Nonlinear Fano Effect in Hybrid Metal-Semiconductor Nanostructures: The Case of Strong Nonlinearity. *Phys. Rev. B* **2011**, *84*, 081405.
25. Chang, D. E.; Sorensen, A. S.; Demler, E. A.; Lukin, M. D. A Single-Photon Transistor Using Nanoscale Surface Plasmons. *Nat. Phys.* **2007**, *3*, 807–812.
26. Akimov, A. V.; Mukherjee, A.; Yu, C. L.; Chang, D. E.; Zibrov, A. S.; Hemmer, P. R.; Park, H.; Lukin, M. D. Generation of Single Optical Plasmons in Metallic Nanowires Coupled to Quantum Dots. *Nature* **2007**, *450*, 402–406.
27. Kolesov, R.; Grotz, B.; Balasubramanian, G.; Stöhr, R. J.; Nicolet, A. A. L.; Hemmer, P. R.; Jelezko, F.; Wrachtrup, J. Wave-Particle Duality of Single Surface Plasmon Polaritons. *Nat. Phys.* **2009**, *5*, 470–474.
28. Reithmaier, J. P.; Sek, G.; Löffler, A.; Hofmann, C.; Kuhn, S.; Reitzenstein, S.; Keldysh, L. V.; Kulakovskii, V. D.; Reinecke, T. L.; Forchel, A. Strong Coupling in a Single Quantum Dot-Semiconductor Microcavity System. *Nature* **2004**, *432*, 197–200.
29. Hennessy, K.; Badolato, A.; Winger, M.; Gerace, D.; Atatüre, M.; Gulde, S.; Fält, S.; Hu, E. L.; Imamoglu, A. Quantum Nature of a Strongly Coupled Single Quantum Dot-Cavity System. *Nature* **2007**, *445*, 896–899.
30. Imamoglu, A.; Woods, H. S. G.; Deutsch, M. Strongly Interacting Photons in a Nonlinear Cavity. *Phys. Rev. Lett.* **1997**, *79*, 1467–1470.
31. Birnbaum, K. M.; Boca, A.; Miller, R.; Boozer, A. D.; Northup, T. E.; Kimble, H. J. Photon Blockade in an Optical Cavity with One Trapped Atom. *Nature* **2005**, *436*, 87–90.

32. Fink, J. M.; Göppl, M.; Baur, M.; Bianchetti, R.; Leek, P. J.; Blais, A.; Wallraff, A. Climbing the Jaynes–Cummings Ladder and Observing Its Nonlinearity in a Cavity QED System. *Nature* **2008**, *454*, 315–318.
33. Koppens, F. H. L.; Chang, D. E.; García de Abajo, F. J. Graphene Plasmonics: A Platform for Strong Light–Matter Interactions. *Nano Lett.* **2011**, *11*, 3370–3377.
34. Jablan, M.; Buljan, H.; Soljačic, M. Plasmonics in Graphene at Infrared Frequencies. *Phys. Rev. B* **2009**, *80*, 245435.
35. Vakil, A.; Engheta, N. Transformation Optics Using Graphene. *Science* **2011**, *332*, 1291–1294.
36. Nikitin, A. Y.; Guinea, F.; García-Vidal, F. J.; Martín-Moreno, L. Fields Radiated by a Nanoemitter in a Graphene Sheet. *Phys. Rev. B* **2011**, *84*, 195446.
37. Novoselov, K. S.; Geim, A. K.; Morozov, S. V.; Jiang, D.; Zhang, Y.; Dubonos, S. V.; Grigorieva, I. V.; Firsov, A. A. Electric Field Effect in Atomically Thin Carbon Films. *Science* **2004**, *306*, 666–669.
38. Novoselov, K. S.; Geim, A. K.; Morozov, S. V.; Jiang, D.; Katsnelson, M. I.; Grigorieva, I. V.; Dubonos, S. V.; Firsov, A. A. Two-Dimensional Gas of Massless Dirac Fermions in Graphene. *Nature* **2005**, *438*, 197–200.
39. Bonaccorso, F.; Sun, Z.; Hasan, T.; Ferrari, A. C. Graphene Photonics and Optoelectronics. *Nat. Photonics* **2010**, *4*, 611–622.
40. Chen, C. F.; Park, C. H.; Boudouris, B. W.; Horng, J.; Geng, B.; Girit, C.; Zettl, A.; Crommie, M. F.; Segalman, R. A.; Louie, S. G.; *et al.* Controlling Inelastic Light Scattering Quantum Pathways in Graphene. *Nature* **2011**, *471*, 617–620.
41. Mak, K. F.; Sfeir, M. Y.; Wu, Y.; Lui, C. H.; Misewich, J. A.; Heinz, T. F. Measurement of The Optical Conductivity of Graphene. *Phys. Rev. Lett.* **2008**, *101*, 196405.
42. Ficek, Z.; Tanas, R. Entangled States and Collective Nonclassical Effects in Two-Atom Systems. *Phys. Rep.* **2002**, *372*, 369–443.
43. Meystre, P.; Sargent, M., III. *Elements of Quantum Optics*; Springer-Verlag: Berlin, 1990.
44. Jaynes, E.; Cummings, F. Comparison of Quantum and Semiclassical Radiation Theories with Application to the Beam Maser. *Proc. IEEE* **1963**, *51*, 89–109.
45. Laussy, F. P.; del Valle, E.; Schrapp, M.; Laucht, A.; Finley, J. J. Climbing the Jaynes-Cummings Ladder by Photon Counting; arXiv:1104.3564v2.
46. Thongrattanasiri, S.; Koppens, F. H. L.; García de Abajo, F. J. Total Light Absorption in Graphene; arXiv:1106.4460v1.
47. Loudon, R. *The Quantum Theory of Light*; Oxford University Press: Oxford, 2000.
48. Kimble, H. J.; Dagenais, M.; Mandel, L. Photon Antibunching in Resonance Fluorescence. *Phys. Rev. Lett.* **1977**, *39*, 691–695.
49. García de Abajo, F. J.; Howie, A. Retarded Field Calculation of Electron Energy Loss in Inhomogeneous Dielectrics. *Phys. Rev. B* **2002**, *65*, 115418.
50. Wunsch, B.; Stauber, T.; Sols, F.; Guinea, F. Dynamical Polarization of Graphene at Finite Doping. *New J. Phys.* **2006**, *8*, 318.
51. Falkovsky, L. A.; Varlamov, A. A. Space-Time Dispersion of Graphene Conductivity. *Eur. Phys. J. B* **2007**, *56*, 281.
52. Thongrattanasiri, S.; Manjavacas, A.; García de Abajo, F. J. Quantum Finite-Size Effects in Graphene Plasmons. *ACS Nano* **2012**, DOI: 10.1021/nn204780e.